

MIMM-X: Disentangling Spurious Correlations for Medical Image Analysis

Louisa Fay^{1,2(✉)}, Hajar Reguigui², Bin Yang², Sergios Gatidis³, and Thomas Küstner¹

¹ Medical Image and Data Analysis, University Hospital of Tübingen, Germany

² Institute for Signal Processing and System Theory, University of Stuttgart, Germany

³ Stanford University, Department of Radiology, Stanford, USA

louisa.fay@med.uni-tuebingen.de

Abstract. Deep learning models can excel on medical tasks, yet often experience spurious correlations, known as shortcut learning, leading to poor generalization in new environments. Particularly in medical imaging, where multiple spurious correlations can coexist, misclassifications can have severe consequences. We propose MIMM-X, a framework that disentangles causal features from multiple spurious correlations by minimizing their mutual information. It enables predictions based on true underlying causal relationships rather than dataset-specific shortcuts. We evaluate MIMM-X on three datasets (UK Biobank, NAKO, CheXpert) across two imaging modalities (MRI and X-ray). Results demonstrate that MIMM-X effectively mitigates shortcut learning of multiple spurious correlations. The code is publicly available¹.

Keywords: Causality, Disentanglement, Shortcut Learning

1 Introduction

Deep Learning (DL) has transformed medical imaging due its power of identifying patterns in the image that are not immediately visible to the human eye, resulting in remarkable success for segmentation, disease detection and diagnosis [16]. However, medical datasets are inherently heterogeneous, influenced by factors such as scanners, acquisition protocols, and patient demographics. These factors introduce spurious correlations, leading DL models to rely on superficial patterns, known as shortcuts, instead of true causal relationships [11, 19, 17]. Consequently, models that perform well within a training domain often fail to generalize to new distributions [5, 13]. For instance, a model trained on a cohort where a disease is more prevalent in male patients may associate the disease with male sex, yielding to biased predictions when applied to mixed-sex populations. In this scenario, instead of learning the true complex anatomical features indicative of the disease, the model exploits a demographic shortcut that leads to

¹ <https://github.com/lab-midas/MIMM-X>

biased decision-making in patient care. In response, causal representation learning aims to address this issue by disentangling causal relationships from spurious correlations to improve robustness under distribution shifts and counterfactual changes. Existing strategies include counterfactual augmentation [20, 21], dataset rebalancing [1, 14], adversarial training [8], and dependence minimization [12, 7].

The previous Mutual Information Minimization Model (MIMM) [7] addressed shortcut learning by disentangling a primary task from a *single* spurious factor by minimizing mutual information (MI). Yet, real-world medical datasets often contain multiple, entangled spurious correlations. To this end, we propose MIMM-X, a framework that simultaneously disentangles and observes a primary task from multiple spuriously correlated factors with minimal computational overhead. We validate MIMM-X across three large-scale medical imaging datasets using two modalities (brain MRI from the German National Cohort (NAKO)[6] and UK Biobank (UKB)[15], and chest X-ray from CheXpert [10]). We demonstrate that MIMM-X mitigates shortcut learning of the primary task and improves generalization across distribution shifts caused by (i) induced spurious correlations and (ii) factors that may naturally act as spuriously correlated factors, without modifying their distribution in our experimental setup.

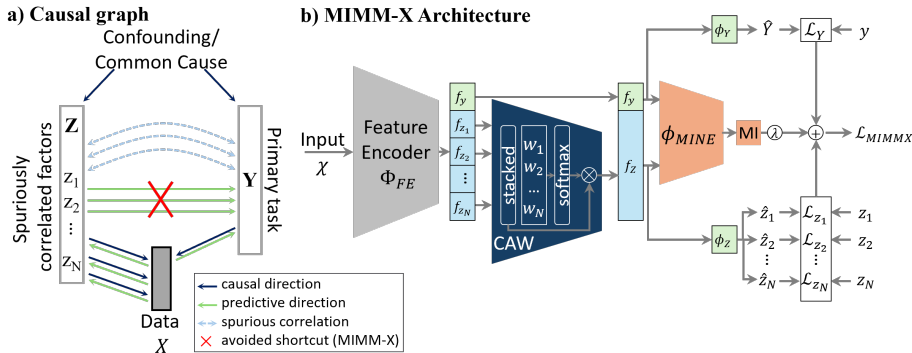


Fig. 1: (a) Causal graph with multiple spurious correlations present. The aim is to avoid predictions based on shortcuts introduced by spurious correlations. (b) Our MIMM-X model promotes causal feature learning by minimizing the MI between the desired primary task y and N spurious correlations Z .

2 Methods

We propose MIMM-X, designed to mitigate multiple spurious correlations $(z_i)_{i=1}^N$ while learning causal representations for a primary task y from a vision input X (Fig. 1a). It is an extension of MIMM [7], which, in comparison, can only handle a single known spurious correlation. As shown in Fig. 1b, MIMM-X consists of a

feature encoder ϕ_{FE} , two classification heads ϕ_Y and ϕ_Z , a mutual information estimator ϕ_{MINE} , and a Confounder Attention Weighter module (CAW).

2.1 Architectural Components

Feature Encoder $\phi_{FE}(X, \theta_{FE})$ maps an image X to a feature vector f , partitioned into $N + 1$ equal-sized subvectors. The subvector f_y encodes the primary task, while $f_Z = [f_{z_1}, \dots, f_{z_N}]^T$ represents the N spuriously correlated factors.

Classification Heads. The primary task y is predicted from f_y through the classification head ϕ_Y with a log-softmax output. All N spuriously correlated factors are predicted from the batch-normalized f_Z with a linear multi-task classification head ϕ_Z and log-softmax.

Confounder Attention Weighter (CAW). Before passing f_z to the classification head ϕ_Z , CAW assigns adaptive attention weights to each spuriously correlated factor. A learnable parameter vector of size N is normalized via softmax to produce attention weights $\mathbf{w} \in \mathbb{R}^N$. Each spuriously correlated feature subvector f_{z_i} is then weighted by its corresponding attention weight w_i to emphasize more relevant spurious factors. The attention weights are learned jointly with ϕ_{FE} .

Mutual Information Estimation ϕ_{MINE} . To enforce independence between f_y and f_Z , we minimize their mutual information (MI). We estimate a single MI value between f_y and the stacked f_Z using a MINE model [2] to keep computational efficiency while scaling to multiple spurious correlations.

2.2 Training Process

MIMM-X uses alternating updates: $\phi_{FE}, \phi_Y, \phi_Z$ and *CAW* are updated on one batch, followed by $N_B - 1$ updates of ϕ_{MINE} where $N_B \in \mathbb{N}$ denotes the number of batches per iteration cycle. The overall loss $\mathcal{L}_{\text{MIMM-X}}$ combines cross-entropy terms \mathcal{L}_0 for y and \mathcal{L}_i for $i = 1, \dots, N$ with MI penalty weighted by λ :

$$\mathcal{L}_{\text{MIMM-X}} = \gamma_0 \mathcal{L}_0 + \sum_{i=1}^N \gamma_i \mathcal{L}_i + \lambda \phi_{MINE}(f_y, f_Z). \quad (1)$$

Inspired by GradNorm [4], task-specific dynamic loss scaling (DLS) adjusts each task's contribution. Scaling factors γ_i are defined as:

$$\gamma_i = \left(\frac{\mathcal{L}_i}{\bar{\mathcal{L}}} \right)^{\alpha_i}, \quad \text{where } \bar{\mathcal{L}} = \frac{1}{N+1} \sum_{i=0}^N \mathcal{L}_i, \quad \text{and } \alpha_i = \begin{cases} \alpha_Y, & \text{if } i = 0, \\ \alpha_Z, & \text{if } i = 1, \dots, N \end{cases} \quad (2)$$

with dynamic α_Y for the primary task:

$$\alpha_Y = \alpha_{Y, \text{initial}} + \left(\frac{\text{epoch}}{N_{\text{epoch}}} \cdot \beta_Y \right), \quad (3)$$

where β_Y controls the increasing emphasis on y over training epochs.

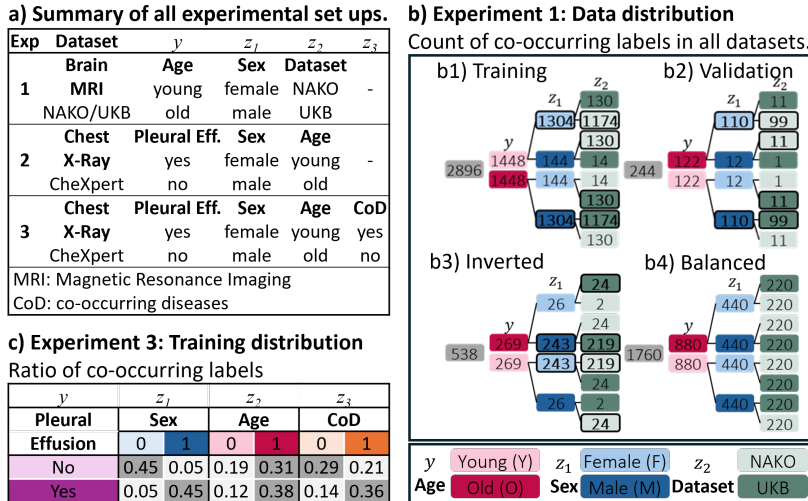


Fig. 2: (a) Summary of experiments, primary tasks y and spurious correlations $(z_i)_{i=1}^N$. (b) Experiment 1: Data distributions (absolute sample counts). (c) Experiment 3: Training data composition with synthetic and natural correlations.

3 Materials

We evaluated MIMM-X in three experiments with two modalities (Fig. 2a).

Training Setup. In Experiments 1–2, we introduced two strong correlations between y and (z_1, z_2) by sub-sampling training data. For each class of y , 90% of samples were drawn from a specific class of z_1 and z_2 , creating spurious correlations between y and z_1, z_2 (see Fig. 2b1). Experiment 3 is based on one synthetic spurious correlation and additionally controls for two potentially naturally occurring spurious correlations (Fig. 2c). All experiments were run on a single NVIDIA GeForce RTX 3090 GPU.

Evaluation. We evaluate all models on three types of datasets: *Validation set* (*Val.*): same spurious correlations as training (Fig. 2b2); *Inverted set* (*Inv.*): inverse correlations (Fig. 2b3); *Balanced set* (*Bal.*): no spurious correlation (Fig. 2b4). If no performance drop is experienced when shifting from the validation distribution to the inverted test distribution, the model successfully avoided learning the shortcut introduced by the spurious correlation.

Evaluation against Comparison Methods. We compare MIMM-X to four methods. *Baseline* uses the same architecture without the MI penalty. *Rebalancing* balances the training set through resampling of under-represented spuriously correlated factor classes. *Distance correlation* (*dCor*) [18, 12] replaces MI with *dCor* as the dependence penalty. *MIMM* [7] minimizes MI between the primary

task and a single spurious factor; we trained separate models for z_1 and z_2 , reporting the mean performance for y and individual results for each z_i .

Evaluation of Disentanglements. We assess cross-predictive performance: using f_y to predict $(z_i)_{i=1}^N$, and $f_{(z_i)_{i=1}^N}$ to predict y on the balanced test set. Ideal disentanglement yields random-guess performance, meaning that no information about the opposed task remains in the specific feature subvector.

Experiment 1 (Brain MRI). We used central 2D axial slices from 3D brain MRI (NAKO/UKB), resized to 256×256 and z-score normalized. As primary task y , we predicted age as binary group (young: <51 years/old: >57 years) from the extracted slice, while we chose z_1 : sex (female/male) and z_2 : dataset (NAKO/UKB) as spuriously correlated factors. We used 2,896 training, 244 validation, 538 inverted, and 1,760 balanced samples (Fig. 2a). We applied the same feature encoder as in [7], which is based on four convolutional layers. Training was performed using a batch size of 150 and $N_B = 6$. DLS hyperparameters are set to $\alpha_Y = 0.3$, $\alpha_Z = 0.8$, $\beta_Y = 0.01$, and $\lambda = 1.5$.

Experiment 2 (Chest X-ray). We used chest X-rays from CheXpert [10] downsampled to 96×96 to predict pleural effusion (yes/no) as primary task y . The training set was strongly correlated by z_1 : sex (female/male) and z_2 : age (young: <50 years/old: >60 years). Our training set included 4,126 X-rays, the validation 408 X-rays, the inverted test set of 2,692 X-rays, and the balanced set 4,432 X-rays. The feature encoder was a DenseNet-121 [9], which was trained for 300 epochs with a learning rate of 10^{-5} and a batch size of 100 using $N_B = 5$. The DLS hyperparameter were $\alpha_Y = 0.3$, $\alpha_Z = 0.7$, $\beta_Y = 0.1$, and $\lambda = 1.5$.

Experiment 3 (Chest X-ray). We extended Experiment 2 to simulate real-world complexity. We kept pleural effusion as primary task y and introduced a single spurious correlation with sex (z_1) in the training set. Additionally, we controlled for two further factors that are often spuriously correlated with disease labels in clinical datasets: age (z_2) and presence of any of the remaining 12 co-occurring lung diseases (CoD, z_3) listed in [3]. These factors were not explicitly correlated with y . Their natural distributions were left unchanged to preserve clinically realistic associations. Importantly, z_2 and z_3 may still act as latent spurious correlates, potentially biasing predictions. This setup enables us to evaluate whether MIMM-X can disentangle y not only from the known spurious factor z_1 , but also from naturally co-occurring variables that are not manually manipulated. The training distribution is shown in Fig. 2c. The dataset included 9,850 training, 1,114 validation, 4,064 inverted, and 2,204 balanced test samples.

4 Results and Discussion

Experiment 1. *Evaluation against Comparison Methods* (Table 1a). In this experiment, we aim to predict age group y from brain MRI based on causal

Table 1: **Experiment 1 (Brain MRI):** Primary task y : age (young/old); spuriously correlated factors z_1 : sex (female/male), z_2 : dataset (NAKO/UKB).(a) **Classification accuracy [%]** across different evaluation sets (Val./Inv./Bal.).

Method	DLS	CAW	$f_y \rightarrow y$			$f_z \rightarrow z_1$			$f_z \rightarrow z_2$		
			Val.	Inv.	Bal.	Val.	Inv.	Bal.	Val.	Inv.	Bal.
Baseline	–	–	96.3	27.2	70.2	99.0	96.4	95.9	100.0	100.0	99.9
Baseline	✓	✓	89.6	42.9	66.6	94.2	91.1	90.5	100.0	100.0	99.8
Rebalance	✓	✓	91.8	81.9	87.3	97.5	96.7	97.3	100.0	100.0	100.0
dCor	–	–	96.2	41.7	73.4	98.8	95.7	96.8	100.0	100.0	99.7
MIMM	–	–	74.4	45.7	58.9	88.3	83.8	85.9	100.0	99.6	99.9
MIMM-X	–	–	46.3	54.0	53.5	89.2	88.3	71.6	99.2	98.3	95.8
MIMM-X	–	✓	94.2	33.2	69.0	63.3	57.5	66.5	54.6	44.5	57.3
MIMM-X	✓	–	85.6	74.2	79.8	96.8	96.3	89.4	98.2	98.4	95.4
MIMM-X	✓	✓	84.2	82.8	82.6	93.4	94.6	93.6	100	99.8	99.5

(b) **Disentanglement performance.** Accuracy in [%]. Ideally, near random (50%).

	Baseline			Rebalance			dCor			MIMM			MIMM-X		
	y	z_1	z_2	y	z_1	z_2	y	z_1	z_2	y	z_1	z_2	y	z_1	z_2
f_y	–	70.3	70.0	–	47.6	48.1	–	70.1	67.4	–	40.4	41.4	–	51.8	50.0
f_{z_1}	51.7	–	51.7	49.6	–	49.4	52.3	–	52.4	54.1	–	–	49.6	–	51.5
f_{z_2}	50.0	50.1	–	50.1	50.0	–	50.1	50.0	–	50.7	–	–	49.8	50.1	–

features, while avoiding shortcuts through induced spurious correlations: sex (z_1) and dataset origin, NAKO or UKB (z_2). We first evaluated the impact of our DLS function (Eq. 2) and CAW module within MIMM-X. Although using CAW without DLS yielded the highest validation accuracy, it dropped by over -60% on the inverted distribution, indicating reliance on spurious correlations (z_1, z_2) that no longer hold in this setting. We found that DLS dynamically balances the loss contributions, preventing the primary task signal from being dominated by easier-to-learn spurious correlations with z_1 and z_2 .

For the comparison methods, Baseline and dCor, performance drops by -61.6% and -54.5% from validation to inverted dataset. The previous model MIMM, designed for a single spurious correlation, also performs poorly in this multi-correlated setting, with performance of y below random guessing on the inverted set. Rebalancing is more robust (-9.9% drop). However, MIMM-X with CAW and DLS effectively prevents shortcut learning and achieves the best generalization, with only a 1.4% performance drop across distributions and the highest accuracy (82.8%) on the inverted set. As expected, the prediction performance of the spuriously correlated factors remains high for all methods and datasets, as these tasks are inherently less complex to learn than age.

Evaluation Disentanglement (Table 1b). We evaluated disentanglement via cross-prediction: predicting z_1/z_2 from f_y and y from f_{z_1}/f_{z_2} to assess residual

shortcut information. Only MIMM-X and Rebalancing achieved near random-guess performance when predicting z_1/z_2 from f_y , confirming effective disentanglement of causal and spurious features. However, compared to MIMM-X, Rebalancing increases the training sample size by 224.3%, requiring more compute and training time. In contrast, Baseline and dCor retained substantial shortcut information. The t-SNE plots (Fig. 3) show that MIMM-X successfully disentangled f_y from sex (z_1) and dataset information (z_2), as no clear separation is visible when coloring f_y by the classes of z_1 (female/male) and z_2 (NAKO/UKB). Other reference methods still allow a separation based on spuriously correlated factors. These results highlight the effectiveness of MIMM-X in mitigating shortcut learning by better disentangling primary features of the age group from spurious correlations of sex and dataset.

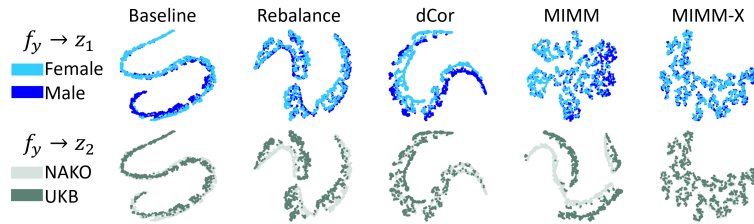


Fig. 3: Experiment 1: t-SNE of f_y colored by spurious factors z_1 : sex, z_2 : dataset. Ideally, f_y is independent of z_1/z_2 , meaning no visual class separation. While reference methods show clusters, MIMM-X is free from spurious information.

Experiment 2. Evaluation against Comparison Methods (Table 2a).

For our CheXpert experiment with two introduced spurious correlations (z_1 :sex, z_2 :age), we expected that shortcut learning is prevented if the performance on inverted and balanced test set for pleural effusion y remained high. Similar to Experiment 1, we found that all comparison methods except for Rebalancing are near 50% on the inverted distribution. Only Rebalancing and MIMM-X generalized well, with MIMM-X achieving the highest inverted accuracy (70.4%).

Evaluation Disentanglement (Table 2b). To evaluate disentanglement, we again predicted y , z_1 , and z_2 from the opposed subvectors, i.e. $f_y \rightarrow z_1/z_2$; $f_{z_1} \rightarrow y/z_2$; $f_{z_2} \rightarrow y/z_1$. Disentanglement results confirmed that MIMM-X and Rebalancing were closest to random guessing across all tasks, while other methods leave substantial spurious information in f_y (accuracies >60%).

Experiment 3. Evaluation against Comparison Methods (Table 3a). In this experiment, we investigated a more realistic setting, where we only induced one spurious correlation, z_1 : sex, while z_2 : age and z_3 : CoD retained as naturally occurring correlations, i.e., their distribution in the training set was left unchanged (Fig. 2c). We found that MIMM-X achieved highest performance on the inverted set with 70.2% for the prediction of pleural effusion. Only Rebalancing achieved

Table 2: **Experiment 2 (X-ray):** Primary task y : pleural effusion; spuriously correlated factors z_1 : sex (female/male), z_2 : age (young/old).

(a) Classification accuracy [%] across different evaluation sets (Val./Inv./Bal.).

Method	$f_y \rightarrow y$			$f_z \rightarrow z_1$			$f_z \rightarrow z_2$		
	Val.	Inv.	Bal.	Val.	Inv.	Bal.	Val.	Inv.	Bal.
Baseline	82.6	42.6	64.0	79.7	74.8	73.6	74.4	70.5	57.4
Rebalance	77.7	70.3	76.4	70.8	69.3	71.2	76.5	71.9	74.8
dCor	87.8	42.2	69.0	80.0	62.3	65.1	83.7	63.8	64.5
MIMM	87.2	51.0	71.4	72.1	68.9	66.7	63.6	64.1	53.1
MIMM-X (ours)	86.3	70.4	76.5	79.1	76.2	77.8	78.2	74.8	77.2

(b) Disentanglement performance. Accuracy in [%]. Ideally, near random (50%).

	Baseline			Rebalance			dCor			MIMM			MIMM-X		
	y	z_1	z_2	y	z_1	z_2	y	z_1	z_2	y	z_1	z_2	y	z_1	z_2
f_y	—	64.5	62.5	—	54.9	53.9	—	66.4	64.0	—	61.1	61.0	—	54.8	54.3
f_{z_1}	57.9	—	55.5	48.8	—	49.4	56.8	—	58.7	49.8	—	—	50.0	—	50.0
f_{z_2}	52.9	62.6	—	52.7	50.5	—	65.8	65.0	—	50.4	—	—	49.6	50.1	—

a similar performance, however, its performance on z_1 and z_2 is below MIMM-X. Other methods showed primary task performance below < 60%.

Evaluation Disentanglement (Table 3b). We evaluated disentanglement again by predicting the opposed task of the subvectors for the primary task and the three spuriously correlated factors. We found that f_y of MIMM-X is closest to random guessing compared to the other comparison methods.

We acknowledge some limitations. MIMM-X currently relies on specifying confounding factors in advance. Extending it to discover unknown spurious correlations automatically and to handle more than three, as well as more complex confounding structures, will be explored in future work. Additionally, while dataset rebalancing can achieve comparable performance in some settings, it requires significantly larger training sets, increasing training time and computational cost. More advanced sampling strategies may mitigate this drawback, but they still rely on explicit knowledge of the spurious attributes and demand careful dataset design. In particular, the latter may not always be achievable in strongly non-homogeneous data cohorts. In contrast, MIMM-X offers a scalable solution that mitigates shortcut learning without modifying the data distribution.

5 Conclusion

This work presents MIMM-X, a scalable method for mitigating multiple spurious correlations and avoiding shortcut learning in DL-based medical image analysis. Our experiments demonstrate that MIMM-X improves robustness and

Table 3: **Experiment 3 (X-ray):** Primary task y : pleural effusion; spuriously correlated factors z_1 : sex (female/male), z_2 : age (young/old), z_3 : CoD (yes/no).

(a) Classification accuracy [%] across different evaluation sets (Val./Inv./Bal.).

Method	$f_y \rightarrow y$			$f_z \rightarrow z_1$			$f_z \rightarrow z_2$			$f_z \rightarrow z_3$		
	Val.	Inv.	Bal.	Val.	Inv.	Bal.	Val.	Inv.	Bal.	Val.	Inv.	Bal.
Baseline	85.4	57.4	71.5	85.7	62.2	58.6	73.2	74.4	73.6	63.5	61.0	62.5
Rebalance	74.2	69.4	71.4	76.8	71.6	74.0	71.7	73.0	72.1	57.7	55.5	57.1
dCor	87.0	54.9	70.9	87.5	72.0	74.0	81.0	80.7	78.0	61.5	57.6	57.5
MIMM-X (ours)	81.7	70.2	72.9	81.5	72.7	74.2	81.4	78.3	79.4	58.9	57.5	58.1

(b) Disentanglement performance. Accuracy in [%]. Ideally, near random (50%).

	Baseline				Rebalance				dCor				MIMM-X			
	y	z_1	z_2	z_3	y	z_1	z_2	z_3	y	z_1	z_2	z_3	y	z_1	z_2	z_3
f_y	—	66.6	60.9	60.3	—	45.7	53.5	50.8	—	70.0	62.2	61.3	—	52.6	53.1	50.9
f_{z_1}	65.9	—	62.8	60.6	68.5	—	62.8	58.5	62.6	—	60.8	59.5	64.7	—	59.9	56.0
f_{z_2}	59.9	59.3	—	57.1	57.1	55.0	—	53.7	57.5	53.8	—	52.5	56.9	53.5	—	52.3
f_{z_3}	55.4	53.9	60.1	—	50.1	50.1	56.2	—	50.0	50.0	56.0	—	50.0	50.0	56.2	—

feature disentanglement in scenarios with both induced and naturally occurring correlations, contributing toward causal and fair predictions.

Acknowledgments. This project was conducted with data (Application No. NAKO-195 and NAKO-708) from the German National Cohort (NAKO) (www.nako.de). The NAKO is funded by the Federal Ministry of Education and Research (BMBF) [project funding reference no. 01ER1301A/ B/C and 01ER1511D], federal states of Germany and the Helmholtz Association, the participating universities and the institutes of the Leibniz Association. We thank all participants who took part in the NAKO study and the staff of this research initiative.

This work was carried out under U.K. Biobank Application 40040. They also thank all participants who took part in the UKB study and the staff in this research program.

Disclosure of Interests. The authors declare no competing interests.

References

1. Ando, S., Huang, C.Y.: Deep over-sampling framework for classifying imbalanced data. In: Machine Learning and Knowledge Discovery in Databases: European Conference, ECML PKDD 2017, Skopje, Macedonia, September 18–22, 2017, Proceedings, Part I 10. pp. 770–785. Springer (2017)
2. Belghazi, M.I., Baratin, A., Rajeshwar, S., Ozair, S., Bengio, Y., Courville, A., Hjelm, D.: Mutual information neural estimation. In: International conference on machine learning. pp. 531–540. PMLR (2018)

3. Chambon, P., Delbrouck, J.B., Sounack, T., Huang, S.C., Chen, Z., Varma, M., Truong, S.Q., Chuong, C.T., Langlotz, C.P.: Chexpert plus: Augmenting a large chest x-ray dataset with text radiology reports, patient demographics and additional image formats. arXiv preprint arXiv:2405.19538 (2024)
4. Chen, Z., Badrinarayanan, V., Lee, C.Y., Rabinovich, A.: Gradnorm: Gradient normalization for adaptive loss balancing in deep multitask networks. In: International conference on machine learning. pp. 794–803. PMLR (2018)
5. Cohen, J.P., Hashir, M., Brooks, R., Bertrand, H.: On the limits of cross-domain generalization in automated x-ray prediction. In: Medical Imaging with Deep Learning. pp. 136–155. PMLR (2020)
6. geschaeftsstelle@ nationale-kohorte. de, G.N.C.G.C.: The german national cohort: aims, study design and organization. European journal of epidemiology **29**(5), 371–382 (2014)
7. Fay, L., Cobos, E., Yang, B., Gatidis, S., Küstner, T.: Avoiding shortcut-learning by mutual information minimization in deep learning-based image processing. IEEE Access **11**, 64070–64086 (2023)
8. Ganin, Y., Lempitsky, V.: Unsupervised domain adaptation by backpropagation. In: International conference on machine learning. pp. 1180–1189. PMLR (2015)
9. Huang, G., Liu, Z., Van Der Maaten, L., Weinberger, K.Q.: Densely connected convolutional networks. In: Proceedings of the IEEE conference on computer vision and pattern recognition. pp. 4700–4708 (2017)
10. Irvin, J., Rajpurkar, P., Ko, M., Yu, Y., Ciurea-Ilcus, S., Chute, C., Marklund, H., Haghgoo, B., Ball, R., Shpanskaya, K., et al.: Chexpert: A large chest radiograph dataset with uncertainty labels and expert comparison. In: Proceedings of the AAAI conference on artificial intelligence. vol. 33, pp. 590–597 (2019)
11. Kumar, A., Fathi, N., Mehta, R., Nichyporuk, B., Falet, J.P.R., Tsafaris, S., Arbel, T.: Debiasing counterfactuals in the presence of spurious correlations. In: Workshop on Clinical Image-Based Procedures. pp. 276–286. Springer (2023)
12. Müller, S., Fay, L., Koch, L.M., Gatidis, S., Küstner, T., Berens, P.: Benchmarking dependence measures to prevent shortcut learning in medical imaging. In: International Workshop on Machine Learning in Medical Imaging. pp. 53–62. Springer (2024)
13. Pooch, E.H., Ballester, P., Barros, R.C.: Can we trust deep learning based diagnosis? the impact of domain shift in chest radiograph classification. In: Thoracic Image Analysis: Second International Workshop, TIA 2020, Held in Conjunction with MICCAI 2020, Lima, Peru, October 8, 2020, Proceedings 2. pp. 74–83. Springer (2020)
14. Sagawa, S., Koh, P.W., Hashimoto, T.B., Liang, P.: Distributionally robust neural networks for group shifts: On the importance of regularization for worst-case generalization. arXiv preprint arXiv:1911.08731 (2019)
15. Sudlow, C., Gallacher, J., Allen, N., Beral, V., Burton, P., Danesh, J., Downey, P., Elliott, P., Green, J., Landray, M., Liu, B., Matthews, P., Ong, G., Pell, J., Silman, A., Young, A., Sprosen, T., Peakman, T., Collins, R.: Uk biobank: An open access resource for identifying the causes of a wide range of complex diseases of middle and old age. PLOS Medicine **12**(3), 1–10 (03 2015). <https://doi.org/10.1371/journal.pmed.1001779>, <https://doi.org/10.1371/journal.pmed.1001779>
16. Suganyadevi, S., Seethalakshmi, V., Balasamy, K.: A review on deep learning in medical image analysis. International Journal of Multimedia Information Retrieval **11**(1), 19–38 (2022)

17. Sun, S., Koch, L.M., Baumgartner, C.F.: Right for the wrong reason: can interpretable ml techniques detect spurious correlations? In: International Conference on Medical Image Computing and Computer-Assisted Intervention. pp. 425–434. Springer (2023)
18. Székely, G.J., Rizzo, M.L., Bakirov, N.K.: Measuring and testing dependence by correlation of distances. *The Annals of Statistics* (2007)
19. Veitch, V., D'Amour, A., Yadlowsky, S., Eisenstein, J.: Counterfactual invariance to spurious correlations: Why and how to pass stress tests. arXiv preprint arXiv:2106.00545 (2021)
20. Xu, M., Zhang, J., Ni, B., Li, T., Wang, C., Tian, Q., Zhang, W.: Adversarial domain adaptation with domain mixup. In: Proceedings of the AAAI conference on artificial intelligence. vol. 34, pp. 6502–6509 (2020)
21. Yao, H., Wang, Y., Li, S., Zhang, L., Liang, W., Zou, J., Finn, C.: Improving out-of-distribution robustness via selective augmentation. In: International Conference on Machine Learning. pp. 25407–25437. PMLR (2022)